



HAL
open science

ONE-DIMENSIONAL MIXTURE MODEL CODE FOR THE MODELING OF TWO-PHASE FLOW THERMOSIPHON

Pierre Boyer, Catherine Colin, Thomas Prusek

► **To cite this version:**

Pierre Boyer, Catherine Colin, Thomas Prusek. ONE-DIMENSIONAL MIXTURE MODEL CODE FOR THE MODELING OF TWO-PHASE FLOW THERMOSIPHON. *Multiphase Science and Technology*, 2023, 35 (4), pp.47-61. 10.1615/MultScienTechn.2023047915 . hal-04837856

HAL Id: hal-04837856

<https://ut3-toulouseinp.hal.science/hal-04837856v1>

Submitted on 16 Dec 2024

HAL is a multi-disciplinary open access archive for the deposit and dissemination of scientific research documents, whether they are published or not. The documents may come from teaching and research institutions in France or abroad, or from public or private research centers.

L'archive ouverte pluridisciplinaire **HAL**, est destinée au dépôt et à la diffusion de documents scientifiques de niveau recherche, publiés ou non, émanant des établissements d'enseignement et de recherche français ou étrangers, des laboratoires publics ou privés.

One-dimensional mixture model code for the modeling of two-phase flow thermosiphon

Pierre Boyer^{a,b}, Catherine Colin^a, Thomas Prusek^b

^aIMFT, Université de Toulouse, CNRS, INPT, UPS, 2 allée Camille Soula, Toulouse, 31400, France

^bEDF R&D, Département MFEE, 6 quai Wattier, Chatou, 78400, France

Abstract

The numerous coupled physical phenomena involved in natural circulation two-phase flow loops make their analytical or numerical modelization difficult. A 1D mixture model code has been developed for the sizing of semi-closed thermosiphon loops. **The results of the code have been compared to existing experimental data of several two-phase flow thermosiphons. A reasonable agreement was found between the experimental and computed mass fluxes. Additionally, a sensitivity analysis was conducted on the pipe diameter, the imposed pressure and the position of the condenser.** The model was finally used to size an experimental thermosiphon loop.

Keywords: two phase flow, natural circulation, thermosiphon loop, heat exchanger

1. Introduction

Passive systems designs are seen as a credible solution for heat removal in many applications, such as the cooling of the containment building in the event of an accident. **In the case of the Fukushima accident, the shutdown of the pumps following the failure of their power supply led to the interruption of core cooling [1].** Indeed, in the case of Loss of Coolant (LOCA) or Main Steam Line Break (MSLB) incident, the temperature and pressure inside the containment building are bound to increase. A type of passive systems, based on a closed thermosiphon loop, is considered for containment cooling: a natural two-phase flow circulation between a heat exchanger placed in a containment and a heat exchanger placed in a water tank.

Numerous studies have been conducted on experimental thermosiphons, the height of those thermosiphons may vary from the less than one meter [2][3], to several meters [4][5][6]. Steady and unsteady behaviors are investigated, since instabilities are likely to occur in two-phase flow and passive systems [7]. Many flow regimes are encountered, such as bubbly, slug, churn and annular flows. In some studies those flow regimes are directly observed through glass surfaces [8]. The evolution of flow rate with heating power is also investigated, and sensitivity studies are run on pipe height or pipe diameter [9], and pressure inside the device [4]. The effects of subcooling and local pressure drop have also been reviewed [10]. **In order to simulate thermosiphons numerically various models have been carried out such as one dimensional homogeneous models [8][11][12] or industrial system codes : RELP5 [13], GOTHIC [4].**

The work presented in this article consists in the development of a model able to accurately size such a system. With the dimensions of the thermosiphon, the heating power and the thermodynamic characteristics of the fluid at the initial stage as input data, the code can compute the mass flow rate, the thermodynamic characteristics of the fluid and the flow regime everywhere in the loop at the steady state, should such a state exists.

2. Model

A thermosiphon is a passive system composed of a heating and a cooling source. The heating source is located below the cooling one, the density of the heated fluid is lower than that of the cooled fluid. The heated fluid hence tends

Email address: pierre.boyer@toulouse-inp.fr (Pierre Boyer)

to flow upward in the thermosiphon, and the cooled fluid flows downward. This creates a natural circulation in the thermosiphon. Such a system is a means for transferring heat between a hot source and a cold source, the circulation induced by natural convection being much more efficient than conduction through a solid. The system being passive, no mechanical work is required for operation (*e.g.* pump, compressor), except possibly for the activation of such a system (active valve to open the system, ...).

The work presented here focuses on a two-phase flow thermosiphon. The geometry is a rectangular loop (Figure 1), the heat source, in red, is named evaporator and its length is l_e . Likewise, the cooling source, named condenser, is represented in blue and its length is l_c . Two configurations are studied, one in which the condenser is located on the vertical downward leg and the other with the condenser on the top horizontal leg. The total height of the loop is H and its width L . The pipe diameter D is uniform.

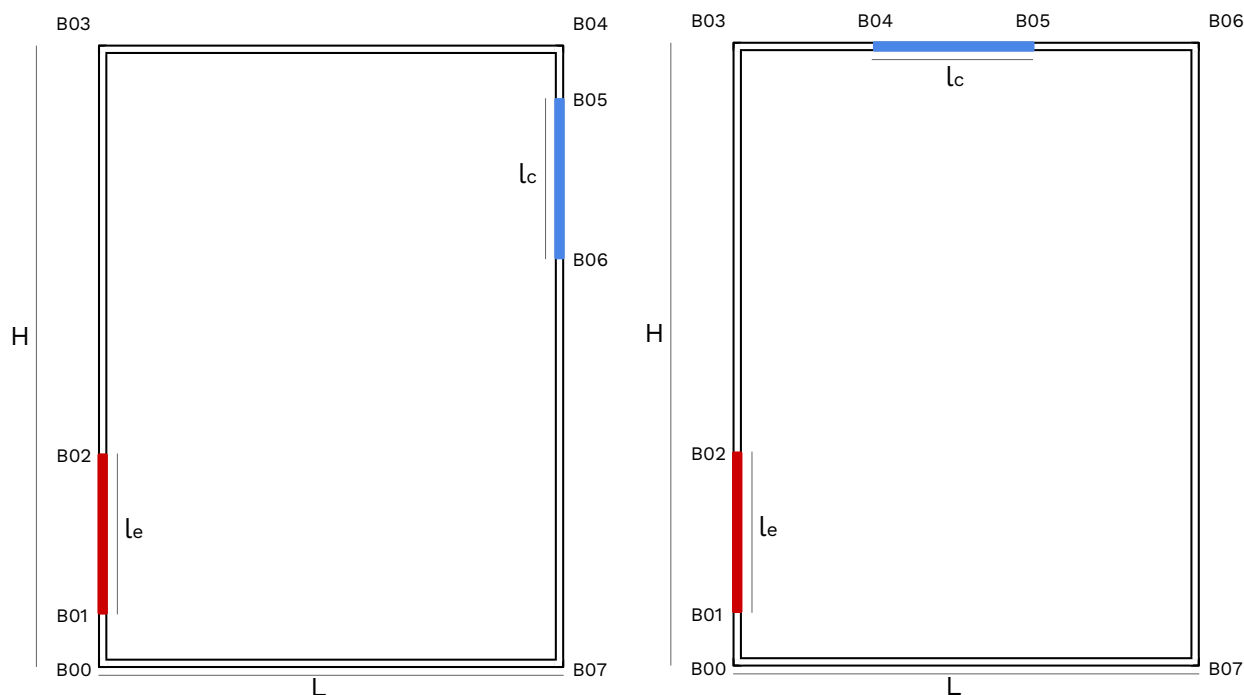


Figure 1: Schematic diagram of a thermosiphon for the vertical (left) and horizontal (right) condenser configurations

2.1. The working principle of a thermosiphon loop

As previously discussed, the difference in density of the fluid in the hot and cold legs generates a driving gravitational force. The gravitational pressure gradient is competing with the frictional pressure gradient. At a functioning regime, an equilibrium between the gravitational pressure drop H_{grav} on height H and the frictional pressure drop H_{fri} is met :

$$H_{grav} + H_{fri} = 0 \quad (1)$$

At such a state, the density distribution in the thermosiphon with a vertical condenser might look like Figure 2. In the evaporator the fluid density decreases due to dilation and phase change, conversely in the condenser the density increases. The density also increases in the tube to simulate heat loss. The gravitational pressure drop generated by the thermosiphon is computed by :

$$\int_0^H (\rho_{down} - \rho_{up})g dz = \int_0^H \Delta\rho g dz \quad (2)$$

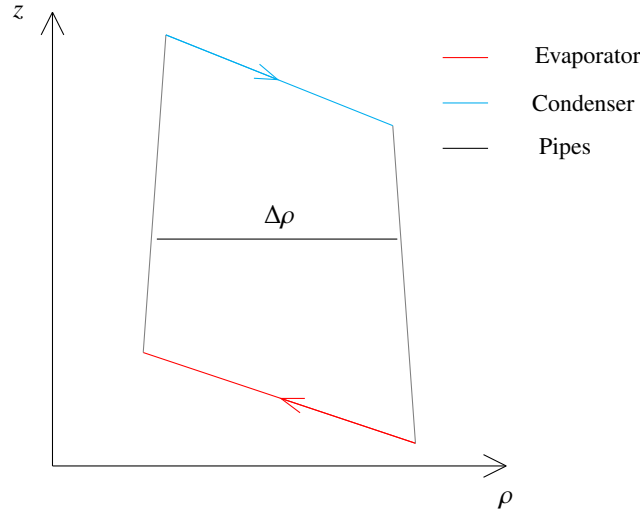


Figure 2: Distribution of density against height inside a thermosiphon

ρ_{down} and ρ_{up} being respectively the mean density at the coordinate z in the downward and upward legs. To increase the gravitational pressure drop, the total height H or $\Delta\rho$ needs to increase also. The shorter the length of the exchangers (for the same heat input/removal) the bigger the $\Delta\rho$. For a thermosiphon with a horizontal condenser, all the fluid is cooled without a change in elevation, which makes it theoretically optimal. However, condensation in a horizontal tube differs from that of a vertical one, the flow might be stratified and the heat exchange demeaned.

Additionally, the energy conservation states that the sum of the imputed heat at the evaporator (Q_i), the heat removed at the condenser (Q_o) and the heat losses (Q_l) must be null. The inputted heat is positive, and its value is greater than the absolute value of the negative removed heat. The heat losses must be minimized.

$$Q_i + Q_o + Q_l = 0 \quad (3)$$

The thermosiphons discussed can be categorized; the first type is the closed configuration, with no openings to the outside pressure, meaning the mass of fluid is conserved. In the semi-closed configuration there is an opening to the outside pressure somewhere in the loop (opened valve at the summit, connection to an expansion vase), mass may hence vary inside the loop. And the open configuration for which the cold source is a free surface water tank. In this work, only semi-closed configuration will be discussed.

2.2. Physical model

The model describes the equations of the water/steam mixture within a semi-closed loop. The loop consists of two heat exchangers, an evaporator at the bottom of the riser and a condenser at the top of downcomer, and pipes between the two. The loop is a rectangle and the diameter is uniform. In order to define a model, the following hypotheses are made :

- The problem is unidimensional
- The two phases are described as a mixture model
- The fluid is always at saturation everywhere in the loop
- Saturation enthalpy does not vary in the exchangers
- All the vapor produced in the evaporator is condensed at the exit of the condenser
- Only two-phase flow regimes are considered

- Only steady state is considered
- No heat losses is considered

In order to run the 1D model for a loop, a periodic boundary condition is imposed at the start and the end of the domain. The fluid being considered at saturation everywhere in the loop, it is not possible to simulate a state in which the liquid is subcooled at the exit of the condenser or the vapor overheated at the exit of the evaporator. Those hypotheses were made in order to simplify the model enough to easily size an experimental thermosiphon. The simplicity of the model allows many computations to be run in a short time. The equations describing the mixture are respectively the conservation of mass, the momentum balance for the mixture and the conservation of enthalpy of the mixture :

$$\frac{\partial G}{\partial z} = 0 \quad (4)$$

$$G^2 \frac{\partial}{\partial z} \left(\frac{(1-x)^2}{\rho_l(1-\alpha)} + \frac{x^2}{\rho_v\alpha} \right) = -\frac{\partial p}{\partial z} + \frac{\tau_p S_p}{A} - (\rho_l(1-\alpha) + \rho_v\alpha)g \sin\theta \quad (5)$$

$$G h_{lv} \frac{\partial x}{\partial z} = \frac{4q_p}{D} \quad (6)$$

G ($kg.m^{-2}.s^{-1}$) being the mass flux, z (m) the axial coordinate, p (Pa) the pressure, τ_p (Pa) the wall friction, S_p (m) the pipe perimeter, A (m^2) the pipe cross-section, ρ_k ($kg.m^{-3}$) the density of phase k , α the void fraction, g ($m.s^{-2}$) the gravitational acceleration, h_{lv} ($J.kg^{-1}$) the phase change enthalpy, x the quality and q_p ($W.m^{-2}$) the heat flux either at the evaporator (positive), the condenser (negative) or the pipes (null). q_p at the evaporator or at the condenser is considered as input data at the evaporator, its absolute value is the heating power divided by the surface area of the exchanger. Depending on whether the simulated thermosiphon is in semi-closed or closed configuration, a pressure condition can respectively be imposed at one point on the loop or be an initial condition.

An additional constraint exists due to the continuity of pressure in the loop, however the mass conservation equation only states that the flow rate is uniform, thus there are 3 constraints for 5 unknowns (G, x, α, τ_p and p). Two closure models must be chosen :

2.2.1. The drift flux model

In order to predict the void fraction, a drift flux model is used. In this model, the velocity of the vapor phase is expressed versus the mixture velocity and a drift velocity U_∞ . The parameter C_0 depends on the local void fraction and velocity profiles. With the vapor phase velocity it is possible to compute the void fraction.

$$U_v = C_0(j_l + j_v) + U_\infty \quad (7)$$

$$\alpha = \frac{Gx}{\rho_v U_v} \quad (8)$$

j_l and j_v are respectively the liquid and vapor superficial velocities. **In vertical upward flow** depending on the flow configuration (bubbly, annular, ...) different correlations can be used to model the coefficient C_0 and the drift velocity U_∞ .

Bubbly flows: Rouhani-Axelson :[14] model

$$U_\infty = 1.18 * \left(g\sigma \left(\frac{\rho_l - \rho_v}{\rho_l^2} \right) \right)^{0.25} \quad (9)$$

$$C_0 = \begin{cases} 1 + 0.2(1-x) \left(\frac{gD\rho_l^2}{G^2} \right)^{0.25} & \text{if } \alpha \leq 0.25 \\ 1 + 0.2(1-x) & \text{otherwise} \end{cases} \quad (10)$$

Slug and churn flows: Ishii [15] model

$$U_{\infty} = \sqrt{2} \left(\frac{\sigma g (\rho_l - \rho_v)}{\rho_l^2} \right)^{0.25} \quad (11)$$

$$C_0 = 1.2 - 0.2 \left(\frac{\rho_v}{\rho_l} \right)^{0.5} \quad (12)$$

Annular flows: Zuber et al.[16] model

$$U_{\infty} = 23 \left(\frac{\mu_l G (1 - x)}{\rho_l \rho_v D} \right)^{0.5} \quad (13)$$

$$C_0 = 1.0 \quad (14)$$

These expressions will be used to calculate the void fraction in the evaporator and the hot leg of the thermosiphon. However, in downward flow the void fraction is typically higher than in upward flow for the same value of quality. According to the flow pattern map of Usui et al. [17], falling film slug flow regime can be observed for the lowest mass fluxes, that is not observed in upward flow. A recent work of Ayegba et al. [18] in vertical upward and downward flow boiling showed that whatever the flow pattern in downward flow, the void fraction is well predicted by the correlation of Rouhani and Axelsson [14]. Therefore whatever the flow regime in the downcomer this correlation will be used to calculate the void fraction.

To determine the flow pattern **in upward flow** and to choose the relevant values of C_0 and U_{∞} , the Mishima and Ishii flow pattern map [19] is used. It gives the flow regime depending on vapor and liquid superficial velocities. **Two criteria** are used to determine the transition from bubbly to slug and churn flow, and from slug and churn flow to annular flow.

Figure 3 displays the regimes observed by Mishima and Ishii on the map of the superficial velocities of vapor j_v and liquid j_l . The authors provide transition criteria. The transition from bubbly to slug/churn is from equations 15. The transition to annular flow is reached for values of j_v superior to the criterion given by equations 16.

$$C = 1.2 - 0.2 \left(\frac{\rho_v}{\rho_l} \right)^{0.5} \quad j_l = \left(\frac{3.33}{C} - 1 \right) j_v - \frac{0.76}{C} \left(\frac{\sigma g \Delta \rho}{\rho_l^2} \right)^{0.25} \quad (15)$$

$$N_{\mu l} = \mu_l \left(\rho_l \sigma \left(\frac{\sigma}{g \Delta \rho} \right)^{0.5} \right)^{-0.5} \quad j_v > \left(\frac{\sigma g \Delta \rho}{\rho_v^2} \right)^{0.25} N_{\mu l}^{-0.2} \quad (16)$$

2.2.2. The wall friction model

For the wall friction, in single-phase flow (mainly liquid) a simple friction coefficient is computed either by Poiseuille (laminar flow) or Blasius (turbulent flow). In two-phase flow the Lockhart-Martinelli model [20] is used.

Single-phase flow:

$$\tau_p = -\frac{1}{2} f_p \rho_k U_k^2 \quad (17)$$

$$f_p = \begin{cases} \frac{64}{Re_k} & \text{if } Re_k < 2300 \text{ (Poiseuille)} \\ 0.3164 Re_k^{-0.25} & \text{otherwise (Blasius)} \end{cases} \quad (18)$$

Two-phase flow:

$$\begin{cases} f_{pl} = K \left(\frac{j_l D}{\nu_l} \right)^{-n} & \{K, n\} = \{16, 1\} \text{ laminar} \\ f_{pv} = K \left(\frac{j_v D}{\nu_v} \right)^{-n} & \{K, n\} = \{0.079, 0.25\} \text{ turbulent} \end{cases} \quad (19)$$

$$X = \frac{j_l}{j_v} \left(\frac{\rho_l f_{pl}}{\rho_v f_{pv}} \right)^{0.5} \quad (20)$$

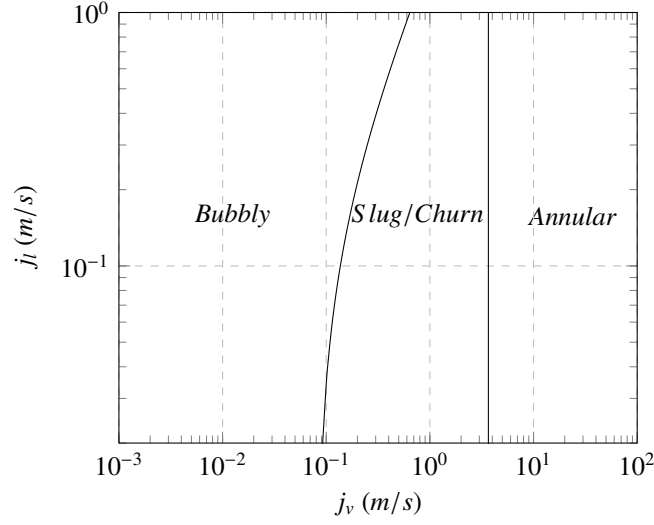


Figure 3: Flow map according to the Mishima [19] criteria for water in a round tube of diameter 11.1 mm at 1 bar

Liquid	Gas	C
Turbulent	Turbulent	20
Laminar	Turbulent	12
Turbulent	Laminar	10
Laminar	Laminar	5

$$\phi_v = (1 + CX + X^2) \quad (21)$$

$$\left(\frac{\partial p}{\partial z}\right)_v = -\frac{S_p}{A} f_{pv} \frac{\rho_v j_v^2}{2} \quad (22)$$

$$\tau_p = \phi_v^2 \frac{A}{S_p} \left(\frac{\partial p}{\partial z}\right)_v \quad (23)$$

2.3. Algorithm

There are now 4 equations (5,6,8 and 17) for 5 unknowns (G, x, α, τ_p and p). The last constraint is the pressure continuity, rather than integrating the pressure on all the domain and trying to solve the system from there, one of the unknown is guessed and the state of the thermosiphon is then computed. The mass flux G is chosen as guessed value since it is uniform in the loop. The pressure continuity is then verified afterward. Indeed, in one point in the loop the pressure is imposed, the pressure elsewhere is computed from this point, the pressure of the last point computed must be equal to the imposed pressure (periodic boundary condition). The validity of the guess value is evaluated by checking whether the pressure continuity is verified. In Figure 4, the overall generated gravitational and frictional pressure drop have been plotted for various choices of G , all other things equal otherwise.

It appears that gravitational pressure drop decreases with the mass flux. Indeed, with an increased mass flux, the quality at the exit of the evaporator is lower (equation 6). The density is hence larger in the hot leg, conversely it is lower in the cold leg (at the same heating power). The frictional pressure drop increase with the mass flux, due to the increase in velocity in both phases. An equilibrium is met, if it exists, at the intersection of the two curves, this is the operating point of the system.

Thus, if the guess value G is wrong, depending whether $H_{grav} > H_{fri}$ or $H_{grav} < H_{fri}$ it is possible to know if the value of G was underestimated or overestimated. The research of the correct G is done by dichotomy: a lower and higher bounds of the mass flux are defined, the value of G is guessed in between those bounds, the state of the

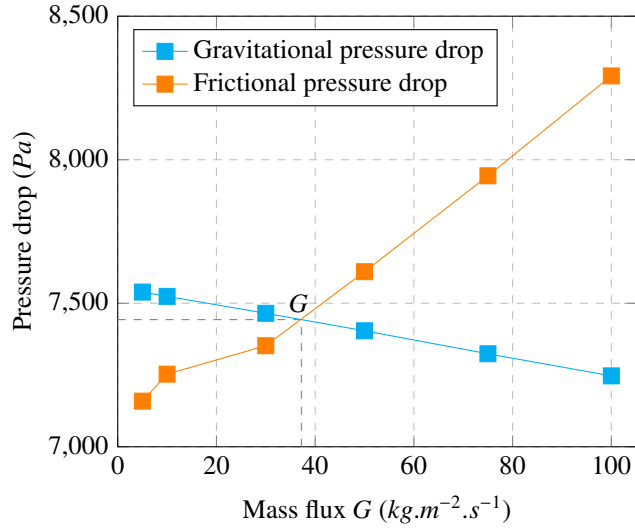


Figure 4: Gravitational and frictional pressure drop against the mass flux in a thermosiphon for a constant heating power (5kW)

loop is then computed. The pressure continuity condition is checked : if the guess value G is too low then it becomes the lower bound, conversely, G becomes the higher bound if overestimated. G is guessed once more, between the updated bound and the state of the loop is computed again. The process is repeated until a mass flux, for which the gravitational and frictional pressure drop are equal, is found. G_l and G_h , defined by the user as an input data, are respectively the lower and higher bounds of the mass flux, x , α , τ_p and p are the unknowns of the system. Figure 5 shows how this algorithm works.

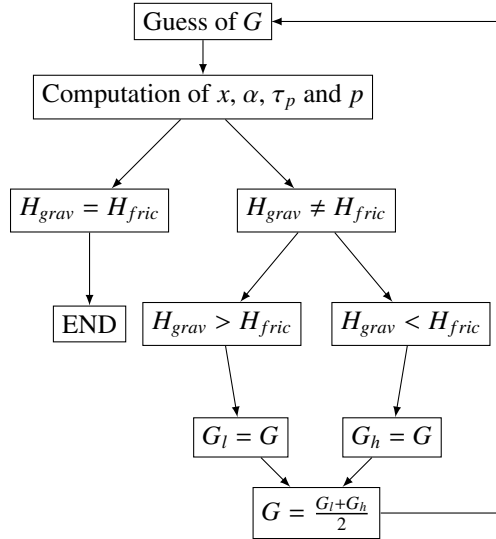


Figure 5: Diagram of the algorithm for the semi-closed configuration

The algorithm is implemented in a *python3* code, equations 5 and 6 are discretized according to a finite differences scheme. The *pyXSteam* [21] is used to access water liquid and vapor properties.

3. Comparison of the experimental data and the model results

Reasonable confidence in the model is needed if it is going to be used for the sizing of an experimental setup. Data from the BARC thermosiphon [22] was used for this purpose. The model is used to simulate the BARC experimental setup and the results are compared to experimental data.

3.1. BARC experimental setup

The available data comes from two different thermosiphon semi-closed loops from the Bhabha Atomic Research Centre (BARC). As seen in Figure 6 the two loops have a different geometry and a steam separator which is not in any configuration presented previously. Indeed, raw data on two-phase flow thermosiphons are scarce and were not found on the exact same configuration as in Figure 1. In this case, vapor is separated from the main loop and condensed in the condenser before going back to the main loop by gravity. **In the model, the length l_c of the condenser is set to 0, the condensation occurs at one point.** Additionally, in one of the loops, an exchanger is located at the exit of the steam separator. It allows subcooling of the liquid. **Since, in the model, the fluid is at saturation temperature everywhere, heat removal without phase change is not possible. The subcooling is hence ignored in the model. The pressure is imposed in the top right corner.** A number of hypotheses on the geometry will be made in order to simulate the two loops with the model. Those are summarized in table 1, the loop of diameter 12.7 mm is named BARC13 and the one of diameter 49.25 mm, BARC49. The working fluid is water.

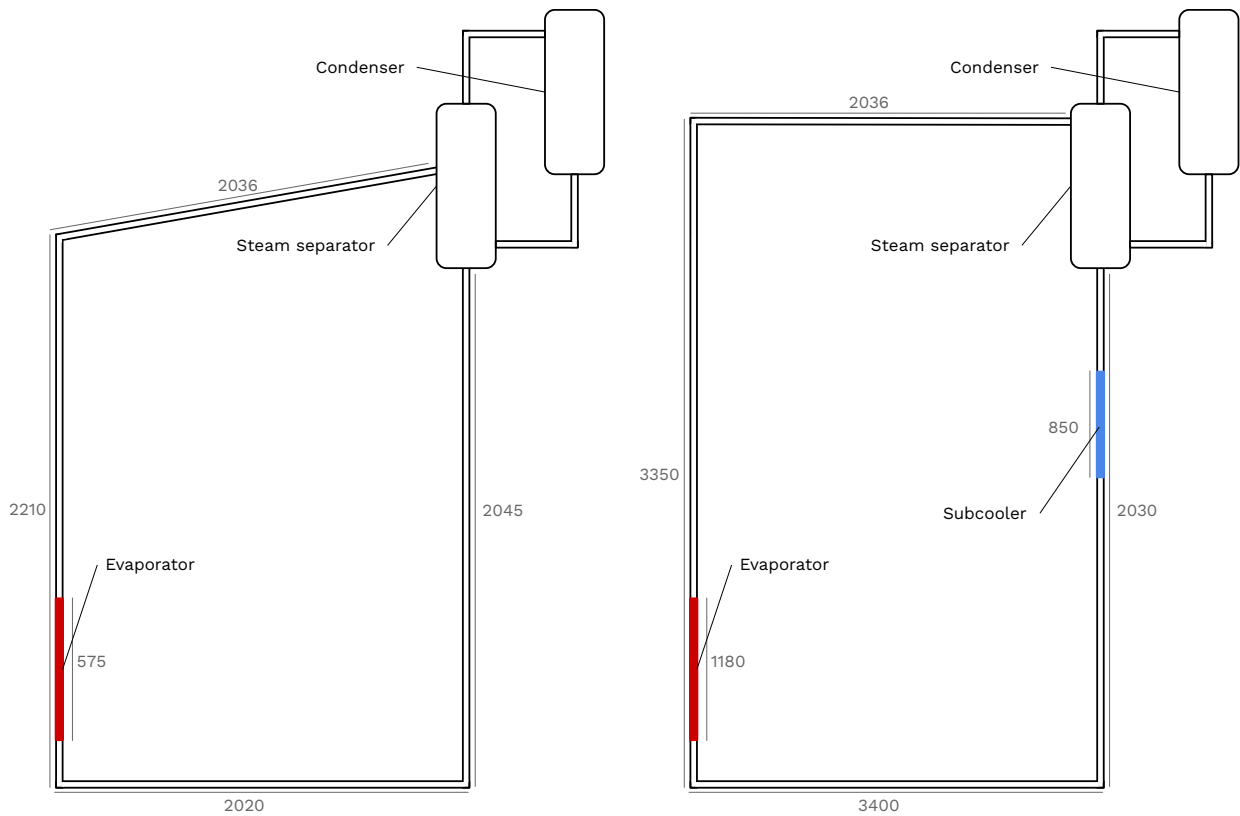


Figure 6: Schematic diagram of a BARC thermosiphons [23] with the 12.7 mm diameter loop on the left and the 49.25 mm diameter loop on the right (all dimensions are in mm)

Height and width are the same in the experimental setups and the model, the same applies to the length of the evaporator. The length of the condenser is considered to be null, the steam separator and condenser are ignored as if the steam was instantly condensed at the location of the condenser. The subcooler is not modeled since no subcooling is possible in the model.

	BARC13	BARC49
D (mm)	12.7	49.25
H (mm)	2210	3350
L (mm)	2020	3400
l_e (mm)	575	1180
l_c (mm)	0	0

Table 1: BARC thermosiphons geometry considered for the model

3.2. Data comparison

The operating pressure as well as the heating power are available in the data of each experimental run. From there, the mass flux is computed for each run by the model. To display the computed data, two additional dimensionless numbers are used, the liquid Reynolds number in the single-phase flow part of the loop (equation 24) and the modified Grashof number (equation 25), the latter comes from the Vijayan et. al article [23]. The Reynolds number is plotted against the modified Grashof number in Figure 7 (a). Lower Gr_m corresponds to BARC13 runs and higher Gr_m to BARC49 runs. For BARC13 the computed and experimental Reynolds curves cross at a Gr_m of 5×10^{12} , and for BARC49 computed Reynolds numbers are underestimated.

$$Re = \frac{GD}{\rho_l \nu_l} \quad (24)$$

$$Gr_m = \frac{4D\rho_l^2\beta gQH}{\pi\mu_l^2 C_{pl}} \quad (25)$$

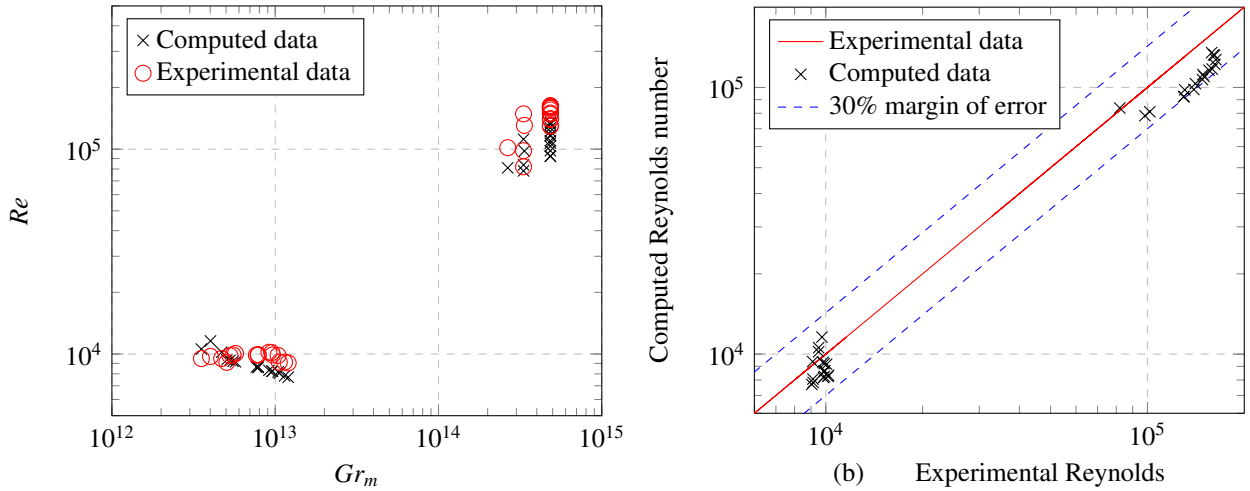


Figure 7: (a) Reynolds against modified Grashof for the BARC experimental data and the model. (b) Computed values of Reynolds against experimental Reynolds values

Q is the heating power (W), ρ_l ($kg.m^{-1}$), μ_l ($Pa.s^{-1}$), ν_l ($m^2.s^{-1}$) and C_{pl} ($J.kg^{-1}$) are properties of water, and β is the dilatation coefficient of water (K^{-1}).

Figure 7 (b) illustrates that the values of the Reynolds numbers computed with the model are within 30% margin of error from experimental values. For the BARC13 loop data, the computed values are both over and under the experimental data curve, as seen previously the mass fluxes are overestimated at low Gr_m and underestimated at high Gr_m . For the BARC49 loop, computed values of Reynolds are almost systematically underestimated. Even though the model is not able to simulate all phenomenons inside the experimental loops, the closeness of the computed mass fluxes and the experimental ones is sufficient for the intended sizing purposes of the model.

4. Model behavior

The model behavior is tested in a square loop, the geometric characteristics of the loop are summarized in table 2. A sensitivity study is conducted on the imposed pressure for the semi-closed model, as well as on the pipes diameter. **The pressure is imposed at the bottom right corner.** For all runs, the working fluid is water.

H	2 m
L	2 m
l_e	0.5 m
l_c	0.5 m

Table 2: Geometry of the modeled loop

For all runs, the pressure P will be imposed on the bottom right of the loop (B07 of figure 1). The sensitivity study will be conducted with the condenser in vertical position. The behavior of the thermosiphon with the condenser in horizontal position will be illustrated.

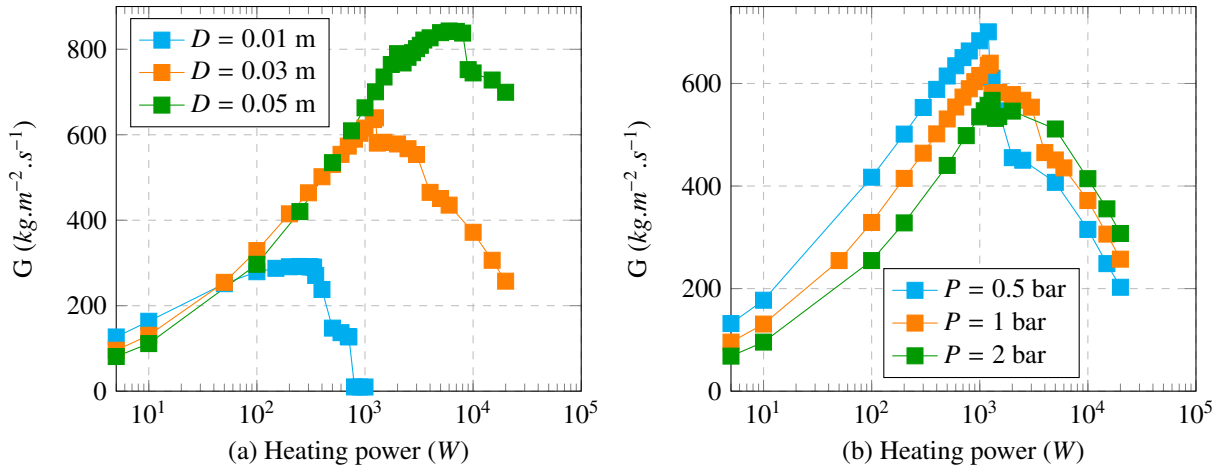


Figure 8: (a) Mass flux against the heating power at 1 bar for several pipe diameters, (b) Mass flux against the heating power in a 3 cm diameter pipe for several imposed pressure

In Figure 8 (a) the mass flux G is plotted against the heating power for several pipes diameter D . Firstly, the mass flux is always larger for larger pipe diameter, since the frictional pressure drop is smaller if the pipe diameter is larger. All three curves go through two regimes: increasing at lower heating power and decreasing as the heating power increases further. In the increasing mass flux regime, an increase in heating power leads to a higher increase in gravitational pressure drop than in frictional pressure drop, it will be referred to as the gravitational regime. The opposite occurs for the decreasing mass flux regime, which will be referred to as the frictional regime. This change in regime occurs because of the variation of the void fraction versus quality. As can be seen on Figure 9, for all drift flux models used in the model, void fraction increases rapidly at low quality and more slowly at high quality. Therefore, for higher void fractions, almost no gravitational pressure drop is generated during heating, while frictional pressure drop keeps on increasing as the fluid velocity increases. This tendency is mitigated as pressure increases.

The profiles of quality, void fraction, pressure as well as the flow regimes are plotted on Figure 10 in a 3 cm diameter pipe. As expected, quality and void fraction increase in the evaporator and decrease in the condenser. The pressure is imposed at the bottom right of the loop (1 bar). From there, since it is at the bottom it can only decrease. Pressure variation is indeed more important in vertical parts. As the heating power increase so does quality and void fraction, pressure on the other hand increases. The flow regimes also differ with the heating power. At lower heating power (200 W) only bubbly flow is observed, as the heating power increases slug, churn (1 kW) and annular (5 kW) flows appear. Annular flow appears out of the exchangers, it can be concluded that it results from the drop in pressure

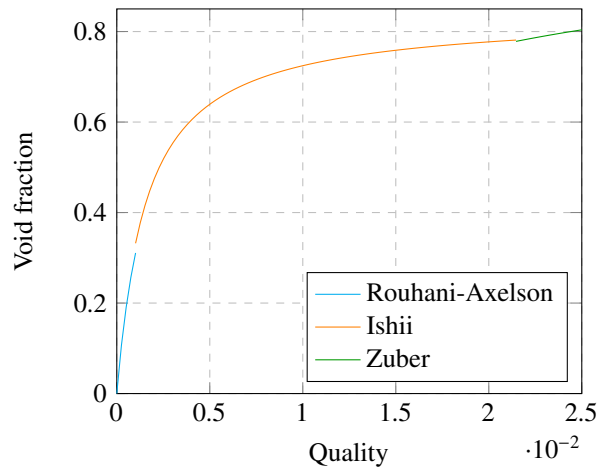


Figure 9: Void fraction against quality for several drift flux model, $G = 100 \text{ (kg.m}^{-2}.\text{s}^{-1}\text{)}$

rather than from heating. The relevance of an annular flow model for horizontal part can be questioned, a stratified model would be more suited. It is a lead for the improvement of the model.

Each plot of Figure 10 corresponds to a point of the orange curves of Figure 8. As can be concluded from their mass fluxes of the three run, the first one (200 W) is in the gravitational regime, the second (1 kW) is at the maximum mass flux and the third (5 kW) is in the friction regime. If the condenser is placed in horizontal position, then as can be seen in Figure 11, the evolution of quality, void fraction and pressure are similar. The flow regimes are also similar to those of the vertical condenser configuration at the same heating power, however, the mass flux is higher. As discussed previously, with the condenser in horizontal position, the void fraction is minimal in all the length of the vertical downward leg. The gravitational pressure drop is hence larger than it is with a vertical condenser. However, heat exchange in a horizontal condenser might not be as good as in a vertical condenser, because of stratified flow.

Finally, for a similar geometry: larger pipes diameter and a horizontal rather than a vertical condenser will allow larger mass fluxes in the loop. Since the goal is to transfer the maximum amount of heat in the thermosiphon, larger pipes diameter will be preferred. Indeed, no mention was made here of critical heat fluxes, but it is doubtful that a 3 cm diameter 50 cm long pipe can be heated up to 20 kW without reaching critical heat flux. At higher mass fluxes, critical heat fluxes will be higher too, a larger heating power will hence be admissible by the evaporator. Additionally, at higher pressures, the mass fluxes are lower in the gravitational regime and larger in the friction regime. Depending on the desired maximum heating power, imposed pressure has to be adjusted so that the maximum heating power coincides with the maximum mass flux, *i.e.* the transition from gravitational to friction regime.

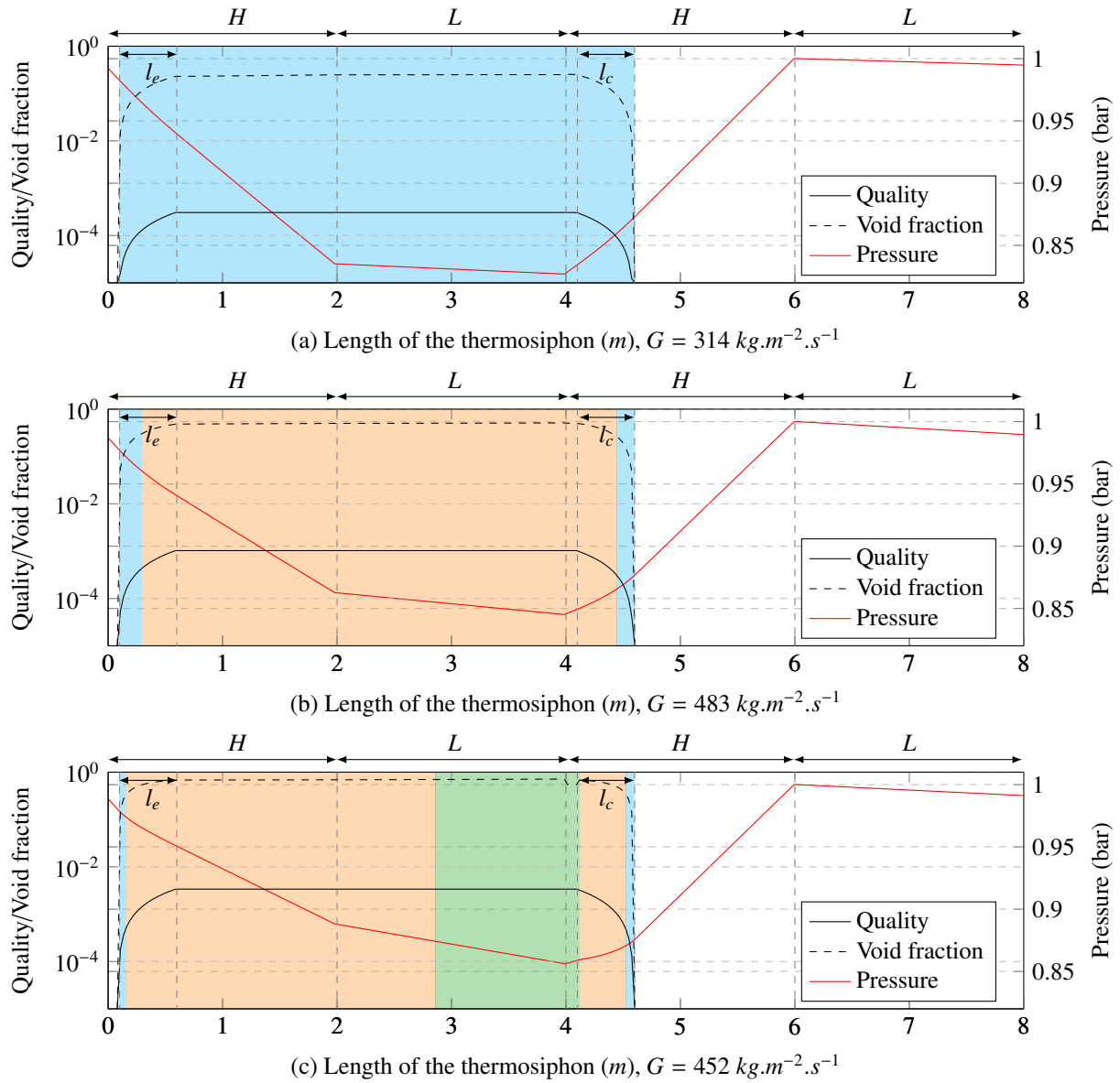


Figure 10: Profile of quality, void fraction and pressure along the length of the thermosiphon with a vertical condenser for a heating power of: (a) 200 W, (b) 1 kW and (c) 5 kW and an imposed pressure of 1 bar in a 3 cm diameter pipe. The color of the background represents the flow regime : white for one phase flow, blue for bubbly flow, orange for slug/churn flow and green for annular flow

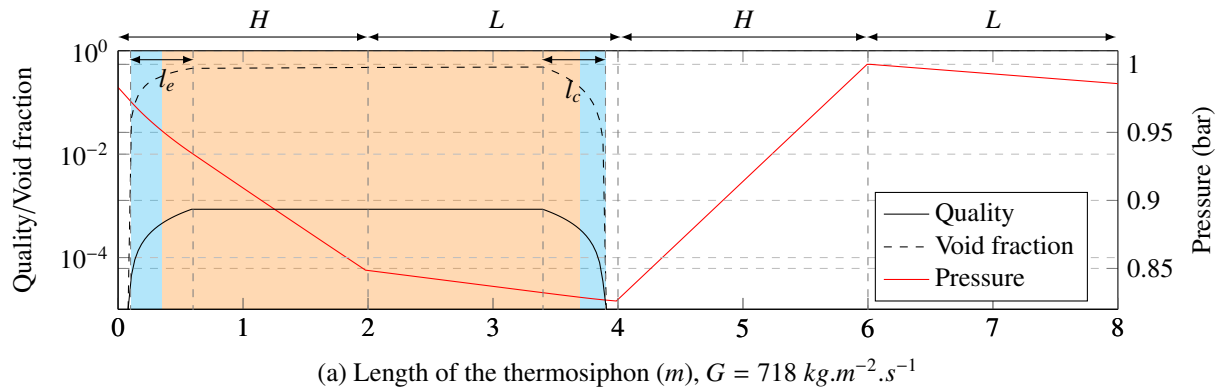


Figure 11: Profile of quality, void fraction and pressure along the length of the thermosiphon with a horizontal condenser for a heating power of 1 kW and an imposed pressure of 1 bar in a 3 cm diameter pipe. The color of the background represents the flow regime : white for one phase flow, blue for bubbly flow, orange for slug/churn flow and green for annular flow

5. Conclusion

A 1D model for two-phase rectangular thermosiphon loop has been developed. The model is able to simulate semi-closed thermosiphons. The semi-closed model has been validated with experimental data. The code has proven to be reasonably reliable, considering the usual margin of error of two-phase natural circulation loops. There is yet still room for improvement in the model, as a model for subcooling and for stratified flow **would be proven useful** for the comparison to experimental data. A sensitivity study was conducted on the semi-closed model. Two functioning regimes were found, a gravitational regime for which the mass flux increases with the heating power and the frictional regime for which it decreases. It appeared that the pipe diameter and imposed pressure had an influence over the mass flux in the loop. Larger pipes diameter yields larger mass fluxes, and larger imposed pressure yields larger mass fluxes in the gravitational regime and lower mass fluxes in the frictional regime. An optimal configuration, in which the mass flux is maximum at the maximum heating power, can hence be found. However, a lack of experimental data available in the literature has made it impossible to validate the code for a fully closed thermosiphon. A sensitivity study was still conducted on the filling ratio. It was found that for larger filling ratios the pressure inside the loop increases rapidly and that a larger heating power was possible at lower filling ratio. The model is also able to simulate thermosiphon loops in closed configuration, however there is still a need of experimental data to validate the model. Thus, to gain confidence in the code for the sizing of a closed thermosiphon an experimental loop is under construction at IMFT, in the frame of a PhD thesis involving IMFT and EDF R&D.

References

- [1] IRSN, L'accident de la centrale nucléaire de Fukushima Daïchi (2011).
- [2] E. R. Fabián, C. M. Ignacio, S. S. Florencio, P. Georgiy, Influencia del flujo de enfriamiento en el comportamiento térmico de un termosifón de contorno, INGENIERÍA MECÁNICA TECNOLOGÍA Y DESARROLLO 5 (2015) 375–384.
- [3] I. Hideaki, S. Yuji, F. Hiromitsu, Flow and heat transfer characteristics in a closed-type two-phase loop thermosyphon (1989).
- [4] L. Changdong, J. Wenyang, Y. Jiang, C. Wei, W. Ting, C. Cheng, X. Hong, Experimental and computational analysis of a passive containment cooling system with closed-loop heat pipe technology, Progress in Nuclear Energy 113 (2019) 206–214. doi:https://doi.org/10.1016/j.pnucene.2019.01.004. URL <https://www.sciencedirect.com/science/article/pii/S014919701930006X>
- [5] X. Yan, G. Fan, Z. Sun, Study on flow characteristics in an open two-phase natural circulation loop, Annals of Nuclear Energy 104 (2017) 291–300. doi:https://doi.org/10.1016/j.anucene.2016.12.038. URL <https://www.sciencedirect.com/science/article/pii/S0306454916311653>
- [6] T. Zhang, Z. J. Ooi, M. Skrzypek, C. S. Brooks, A multi-dimensional dataset for two-phase instability in low pressure natural circulation based on direct transient local measurement, International Journal of Heat and Mass Transfer 151 (2020) 119447. doi:https://doi.org/10.1016/j.ijheatmasstransfer.2020.119447. URL <https://www.sciencedirect.com/science/article/pii/S0017931019351841>
- [7] L. E. O'Neill, I. Mudawar, Review of two-phase flow instabilities in macro- and micro-channel systems, International Journal of Heat and Mass Transfer 157 (2020) 119738. doi:https://doi.org/10.1016/j.ijheatmasstransfer.2020.119738. URL <https://www.sciencedirect.com/science/article/pii/S0017931019328571>

- [8] R. Swart, R. Dobson, Thermal-hydraulic simulation and evaluation of a natural circulation thermosyphon loop for a reactor cavity cooling system of a high-temperature reactor, *Nuclear Engineering and Technology* 52 (07 2019). doi:10.1016/j.net.2019.07.031.
- [9] V. Krishnan, D. Saha, M. R. Gartia, Effect of loop diameter on the steady state and stability behaviour of single-phase and two-phase natural circulation loops, *Science and Technology of Nuclear Installations* 2008 (01 2008). doi:10.1155/2008/672704.
- [10] M. K. Jong, Y. L. Sang, Experimental observation of flow instability in a semi-closed two-phase natural circulation loop, *Nuclear Engineering and Design* 196 (2000) 359–367.
- [11] M. R. Gartia, V. Krishnan, D. Pilkhwal, A generalized flow correlation for two-phase natural circulation loops, *Nuclear Engineering and Design* 236 (2006) 1800–1809. doi:10.1016/j.nucengdes.2006.02.004.
- [12] X. Guo, Z. Sun, J. Wang, S. Yu, Steady-state performances and scaling analyses for an open flashing-driven natural circulation system, *Progress in Nuclear Energy* 87 (2016) 1–14. doi:https://doi.org/10.1016/j.pnucene.2015.11.007.
URL <https://www.sciencedirect.com/science/article/pii/S0149197015301086>
- [13] X. Hou, Z. Sun, W. Lei, Capability of relap5 code to simulate the thermal-hydraulic characteristics of open natural circulation, *Annals of Nuclear Energy* 109 (2017) 612–625. doi:https://doi.org/10.1016/j.anucene.2017.06.010.
URL <https://www.sciencedirect.com/science/article/pii/S0306454916308520>
- [14] S. Rouhani, E. Axelsson, Calculation of void volume fraction in the subcooled and quality boiling regions, *International Journal of Heat and Mass Transfer* 13 (2) (1970) 383–393. doi:https://doi.org/10.1016/0017-9310(70)90114-6.
URL <https://www.sciencedirect.com/science/article/pii/0017931070901146>
- [15] M. Ishii, One-dimensional drift-flux model and constitutive equations for relative motion between phases in various two-phase flow regimes, *Tech. rep.*, Argonne National Lab., Ill.(USA) (1977).
- [16] N. Zuber, F. Staub, G. Bijwaard, P. Kroeger, Steady state and transient void fraction in two-phase flow systems. final report for the program of two-phase flow investigation. volume i., *Tech. rep.*, General Electric Co., Schenectady, NY Research and Development Center (1967).
- [17] K. USUI, Vertically downward two-phase flow, (ii), *Journal of Nuclear Science and Technology* 26 (11) (1989) 1013–1022. doi:10.1080/18811248.1989.9734422.
- [18] P. O. Ayegba, J. Sebilliau, C. Colin, Hydrodynamics of vertical upward and downward flow boiling in a millimetric tube, *International Journal of Multiphase Flow* 153 (2022) 104120. doi:https://doi.org/10.1016/j.ijmultiphaseflow.2022.104120.
URL <https://www.sciencedirect.com/science/article/pii/S0301932222001197>
- [19] K. Mishima, M. Ishii, Flow regime transition criteria for upward two-phase flow in vertical tubes, *International Journal of Heat and Mass Transfer* 27 (5) (1984) 723–737. doi:https://doi.org/10.1016/0017-9310(84)90142-X.
URL <https://www.sciencedirect.com/science/article/pii/001793108490142X>
- [20] V. P. Carey, *Liquid-vapor phase-change phenomena: an introduction to the thermophysics of vaporization and condensation processes in heat transfer equipment*, CRC Press, 2020.
- [21] pyxsteam 0.4.9, <https://pypi.org/project/pyXSteam/>.
- [22] N. Kumar, Rajalakshmi, Kulkarni, Sagar, Vijayan, Saha, Experimental investigations in high-pressure natural circulation loop: progress report for the period january-june, 1999 (2000).
- [23] P. K. Vijayan, A. K. Nayak, D. Saha, M. R. Gartia, Effect of loop diameter on the steady state and stability behaviour of single-phase and two-phase natural circulation loops, *Science and Technology of Nuclear Installations* 2008 (2008) 672704. doi:10.1155/2008/672704.
URL <https://doi.org/10.1155/2008/672704>